The Journal of Undergraduate Research in Physics

CONTENTS

ASYMPTOTIC BEHAVIOR OF DIFFUSION ON RANDOM LATTICES BELOW THE PERCOLATION THRESHOLD.....23

Carola Fassnacht
Universität zu Köln , Köln West Germany

TEMPERATURE INDUCED VALENCE TRANSITIONS IN $SmS_{1-X}P_X$ ALLOYS.....27

K.D. Aylesworth, D.M. Howarth, and M.L. Wallner
University of Wisconsin-Stevens Point, WI

OPTICAL LEVITATION.....31

Donn Michael Silberman
University of Arizona, Tuscon, AZ

LAPLACE'S EQUATION, MICROCOMPUTERS, AND THE CLASSROOM.....37

Jeanne A. Jackson
Appalachian State University, Boone, NC

VOLUME 2, NUMBER 2

OCTOBER, 1983

Published by Guilford College
for
The American Institute of Physics and The Society of Physics Students

THE JOURNAL OF UNDERGRADUATE RESEARCH IN PHYSICS

This journal is devoted to research work done by undergraduate students in physics and its related fields. It is to be a vehicle for the exchange of ideas and information by undergraduate students. Information for students wishing to submit manuscripts for possible inclusion in the Journal follows.

ELIGIBILITY

The author must have performed all work reported in the paper as an undergraduate. The subject matter of the paper is open to any area of pure or applied physics or physics related field.

SPONSORSHIP

Each paper must be sponsored by a full-time faculty member of the department in which the research was done. A letter from the sponsor to the editor must accompany the manuscript if it is to be considered for publication.

FORM

The manuscript should be typed, double spaced, on 8 1/2 x 11 inch sheets. Margins of about 1 1/2 inch should be left on the top, sides, and bottom of each page. Papers should be limited to twelve pages of text in addition to an abstract and appropriate drawings, pictures, and tables.

GENERAL STYLE

All papers must conform to the Style Manual of the American Institute of Physics. Each paper must be prefaced by an abstract that does not exceed 250 words.

ILLUSTRATIONS

Line drawings should be made with black India ink on plain white paper. If a graph is drawn on co-ordinate paper, the paper must be lined blue. Important lines should be ruled in black. Each figure or table must be on a separate sheet. Photographs must have a high gloss finish.

CAPTIONS

A brief caption should be provided for each illustration or table, but it should not be part of the figure. They should be listed together at the end of the manuscript.

EQUATIONS

Equations should appear on separate lines and may be written in black India ink.

FOOTNOTES

Footnotes should be typed double spaced and grouped together in sequence at the end of the manuscript.

SUBMISSION

Two copies of the manuscript should be sent to:

Dr. Rexford E. Adelberger, Editor
THE JOURNAL OF UNDERGRADUATE RESEARCH IN PHYSICS
Physics Department
Guilford College
Greensboro, NC 27410

SUBSCRIPTION INFORMATION

The Journal will be published biannually with issues appearing in April and October of each year. There will be two issues per volume.

TYPE OF SUBSCRIBER	PRICE PER VOLUME
Individual	$ 5.00
Institution	$10.00

Foreign subscribers add $2.00 for postage

To receive a subscription, send your name, address, and check made out to The Journal of Undergraduate Research in Physics (JURP) to:

Journal of Undergraduate Research in Physics
Physics Department
Guilford College
Greensboro, NC 27410

BACK ISSUES

Back issues may be purchased by sending $10.00 per volume to the editorial office.

ISSN 0731 - 3764

The Journal of Undergraduate Research in Physics is published by Guilford College for the American Insititute of Physics and the Society of Physics Students.

A NOTE FROM THE EDITOR ABOUT THE BENDIX AWARDS

For a number of years the Society of Physics Students and Sigma Pi Sigma have given small awards for research done by the various chapters. This has been funded by a grant from the Bendix Corporation. The aim of these awards is to encourage the SPS chapters to engage in some research project that would involve a number of its members. The grant requests can be submitted by any SPS chapter and can be as large at $750.

It appears to me that many students in the various chapters are unaware of the Bendix awards program. It is an ideal place to request support for undergraduate research projects. Has your chapter applied for one? Do you know how to apply? Your chapter advisor has the information about these awards.

One of the papers in this issue was supported by a Bendix Award. It seems most fitting that this work should be published in the research journal of the Society of Physics Students.

As a way of saying congratulations to those chapters that submitted the winning proposals and making the SPS members more aware of the program, we are publishing the abstracts and/or titles of the winning awards for the 1983 - 1984 year.

BENDIX AWARD WINNERS 1983-1984

A VISIBLE LIGHT DOPPLER VELOCIMETER INTERFACED TO A MICROCOMPUTER

East Carolina University Chapter

The Society of Physics Students at East Carolina University proposes to build a Doppler velocimeter using a small Ne-He laser and a microcomputer. The velocimeter then will be used as a demonstration experiment in the Physics Department and as a tool for measuring the velocity of air track carts in the sophomore lab sequence.

MEASUREMENT OF THE EFFECT FERROFLUIDS ON POLARIZED LIGHT

Georgia Institute of Technology

A COMPUTER INTERFACING PROJECT TO IMPROVE THE UTILITY AND SENSITIVITY OF A CONVENTIONAL NUCLEAR MAGNETIC RESONANCE SPECTROMETER

Iona College Chapter

This proposal describes an activity which will merge the interests of the three major segments of undergraduate physical science students at Iona College. We propose to couple the output of a conventional nuclear magnetic resonance spectrometer to available micro and minicomputers. A student designed interface will couple the spectrometer to a microprocesssor used as a data-logger and intermediate storage device. Transfer of the data to a computer will permit data analysis with emphasis on maximization of the signal to noise ratio for signals from low concentration solutions of organic molecules which are of interest to members of the Chemistry and Biology faculties. Design of the data handling system, selection of the best computer from those available and the writing of software are all components of this project.

EVALUATION OF A LARGE DIFFERENTIAL EXPANSION CAPACITANCE THERMOMETER

Jacksonville University Chapter

This project investigates the performance of a three terminal ultra-sensitive capacitance thermometer conceived, designed, and constructed by two SPS members in 1982-1983 to study low temperature transitions in ferroelectrics. We expect to detect temperature changes of 1 micro degree Kelvin using a sensitive capacitance bridge and the large differential expansion between NILO and copper.

CONSTRUCTION OF A TUNABLE DYE LASER FOR USE WITH A NITROGEN LASER

Southern Oregon State College Chapter

To construct a tunable dye laser in conjunction with our nitrogen laser. The dye laser may be tuned to excite selectively any given transition within the wavelength of available dyes. The transitions will be observed and studied experimentally by physicists and the general public.

SOLAR LASER

SUNY Oneonta Chapter

The purpose of the experiment proposed by our SPS chapter is to build a continuous solar pumped laser. This laser will be of the type described in a recent NASA Technical Brief on the subject of solar powered lasers. Our experiment will use an ultra-violet lamp to simulate the ultra-violet band of the sun. We plan to use recently acquired minicomputers and an analog-to-digital converter to automatically collect and interpret the

output of our laser and our photovoltaic cells.

WEATHER SATELLITE RECEIVING STATION
Thiel College Chapter

The Society of Physics Students at Thiel College proposes to expand and update their current earth satellite receiving station by designing and developing a weather satellite receiving station. The main design would be a display method for WEFAX transmissions from the GOES satellites. Several systems are presently under study. These include the use of a modified oscilloscope, facsimile machine and digital scan system. The main item to be purchased will be the S-band downconverter. The project will focus attention on the SPS and our environmental sciences program and lead to a number of student projects.

ANGULAR MOMENTUM OF AN ELECTRIC CURRENT IN A SUPERCONDUCTING LOOP
Washington University Chapter

Using a superconducting current loop as a torsional pendulum, we intend to demonstrate that current carrying electrons have momentum. We will observe qualitatively and quantitatively the mechanical resonance caused by a current which varies at the resonant frequency of a torsional pendulum.

ASYMPTOTIC BEHAVIOR OF DIFFUSION ON RANDOM LATTICES BELOW THE PERCOLATION THRESHOLD

Carola J. Fassnacht
Luxemburger Str. 426
5000 Köln 41
West Germany

ABSTRACT

The asymptotic behavior of diffusion on a random lattice below the percolation threshold was investigated using computer modeling. Deviations from an assumption of Mitescu and Rossenq (Annals of Israel Physics Society 5, 81 (1983)) were found.

INTRODUCTION

This research deals with the "ant in a labyrinth" problem. Imagine a lattice that has the structure of a chess board, but in three dimensions. This lattice consists of many cubes called "sites". These sites are either free or occupied. The lattice as a whole has a concentration of occupied sites p, but the distribution of occupied sites within the lattice is completely random.

Now imagine that an ant is placed in the lattice. The ant can only stay on the occupied sites. If it wished to "walk", it must pass from one occupied site to one of the six nearest-neighbor sites which is also occupied. Thus pathways will be formed along which the ant can walk, pathways created by clusters of occupied sites. Examples of such clusters are shown in Figure 1.

For low concentrations ($p < 1$), the clusters of adjoining sites will be small. This allows the ant only a small range within which to walk. For concentrations near $p = 1$ (almost all sites occupied) there will be one continuous cluster with only a few holes in it. The pathway for the ant then stretches across the whole lattice. Somewhere between these concentrations lies a critical concentration p_c where there are many clusters of occupied sites, and one of them reaches from one end of the lattice to the other. In an infinite lattice, this would be an infinite cluster.

It has been proven rigorously (1) that in a lattice there is either zero, one, or an infinite number of infinite clusters. There are never two or three, etc. infinite clusters. This concentration p_c (called the percolation threshold) is the concentration at which exactly one infinite cluster exists.

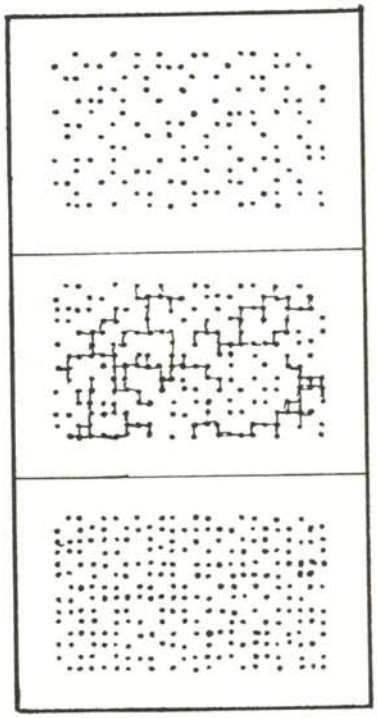

FIGURE 1
Clusters in a small two-dimensional lattice.

To examine the diffusion in the lattice, one allows the hypothetical ant to "walk" randomly through the lattice.

This means that the ant moves with equal likelihood in all six directions. The ant is allowed to walk a while and then its displacement R(t) from the place where it started to walk is measured. One time-unit is the time that the ant needs to walk from one occupied site to the next (or to attempt to walk in that direction if there is no occupied site there).

To obtain statistical values for R(t), a computer simulation was used. A large number of ants are put into the simulated lattice. They are allowed to "walk" around and their average displacement at various times measured. The average of $R^2(t)$ is taken to eliminate the vector character of the displacement. It is the aim of the investigation to describe the average square displacement $\langle R^2(t) \rangle$ as a function of time.

The data is analyzed by examining graphs of $\langle R^2(t) \rangle$ as a function of the concentration. Earlier studies (2) have shown that the graphs take on three different forms. For $p > p_c$ the graph asymptotically approaches a straight line. For $p = p_c$, it approximates the shape of a parabola. For $p < p_c$, it asymptotically approaches a constant

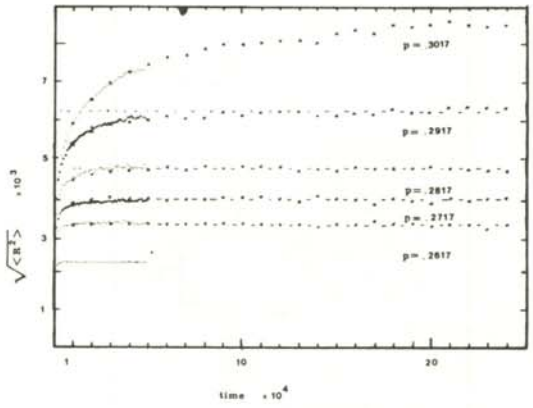

FIGURE 2
Root-mean-square of the displacement versus time.

value (Figure 2). The asymptotic value (R^2_∞) would be reached when all the ants have visited all sites in their clusters with equal probability. The aim of this research is to find the function $\langle R^2(t) \rangle$ for $p < p_c$ from the computer data of Pandey and Stauffer (4).

METHODS

It has been assumed that the graph of $\langle R^2(t) \rangle$ vs time converges exponentially as do most random time-dependent functions. Thus it follows the equation:

$$\langle R^2(t) \rangle = R_\infty - \eta \exp(t/a)$$

where η and a are variables. Theoretical considerations indicate that the time has an exponent x whose value might not be equal to one. (3) This is due to the fact that one does not examine just one cluster, but takes the average over all the clusters in the lattice.

To check the correctness of this equation and to obtain a value for x, the equation is written in a different form:

$$R^2(t) = R^2_\infty - \eta \exp(-t^x/a^x)$$

percolation threshold p = 0.3117

Quality	Range and Step Size
	p=0.2317
(1)	t=100 to t=4900 in steps of 100
(2)	t=1000 to t=49000 in steps of 1000
	p=0.2617 : p=0.2717 : p=0.2817
(1)	t=100 to t=4900 in steps of 100
(1)	t=1000 to t=49000 in steps of 1000
(3)	t=10000 to t=240000 in steps of 10000
	p=0.2917
(1)	t=100 to t=4900 in steps of 100
(1)	t=1000 to t=49000 in steps of 1000
(3)	t=10000 to t=240000 in steps of 10000
(5)	t=100000 to t=900000 in steps of 100000
	p=0.3017
(1)	t=100 to t=4900 in steps of 100
(1)	t=1000 to t=49000 in steps of 1000
(2)	t=10000 to t=240000 in steps of 10000
(4)	t=100000 to t=4900000 in steps of 100000

QUALITY OF THE DATA
LATTICE SIZE = 180 x 180 x 180

(1)	500 ants on each of 20 lattices
(2)	200 ants on each of 20 lattices
(3)	100 ants on each of 20 lattices
(4)	20 ants on each of 10 lattices
(5)	10 ants on each of 10 lattices

TABLE 1
Quality of the data used in determining x. The larger the lattice size, the number of ants, and the number of lattices, the better the quality of the data.

Thus

$$\ln(R^2_\infty - \langle R^2(t) \rangle) = \ln(\eta) - t^x/a^x .$$

Making the substitution:

$$\ln(\Delta) = \ln(R^2_\infty - \langle R^2(t) \rangle) ,$$

yields the equation:

$$\ln(\Delta) = \ln(\eta) - t^x/a^x .$$

If this equation is correct, the graph of $\ln(\Delta)$ versus t should be a straight line.

A qualitative discussion of the data used is presented in Table 1. The larger the lattice size, the number of ants, and the number of lattices, the better the quality of the data. The limiting factor on the quality is the computer time needed to generate the data.

DISCUSSION OF RESULTS

A plot of $\ln(\Delta)$ versus t with a concentration p=0.2917 produced a graph which curved rather strongly. This meant that the value of x was certainly not 1. The plot of $\ln(\Delta)$ versus t was done for a number of values of x until two graphs resulted which were hardly curved, one slightly convex and the other slightly concave (Figure 3). The value of the exponent then must be between 0.47 and 0.45.

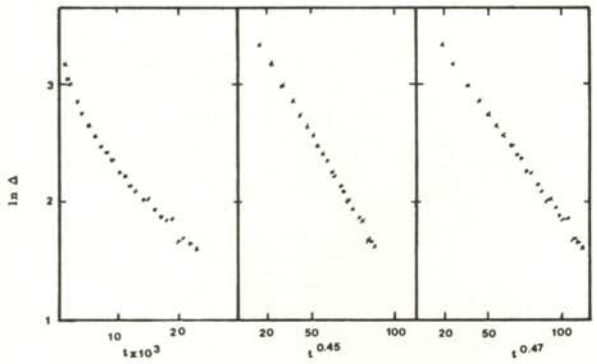

FIGURE 3
Graphical determination of the exponent x with p=0.2917.

The concentrations p = 0.2817 and p = 0.2617 could not be analyzed in this manner for convergance towards R_∞ because the data from the simulation for t=1000 ... t=49,000 converged toward a value which was higher than R_∞ as calculated using the data for t=50,000 ... t=240,000. However, this plotting method used with other concentrations confirmed that x<1 (see Figure 4).

These graphs suggest that for concentrations less than the percolation threshold ($p < p_c$), the values of the average square displacement $\langle R^2(t)\rangle$ converges towards R_∞ according to the relationship:

$$\langle R^2(t)\rangle = R_\infty^2 - \eta \exp -(t/a)^x$$

where $x = 0.4 \pm .1$.

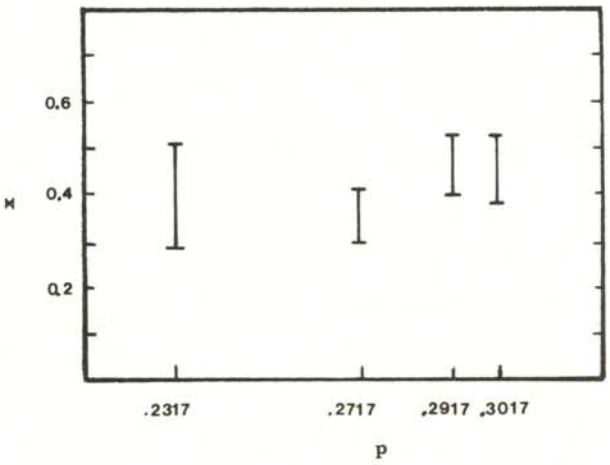

FIGURE 4
Variations of x with various concentrations.

APPLICATION OF THE PROBLEM

The hypothetical problem of an ant walking through a cluster in a lattice can be applied, for example, to determine the electrical conductivity of an alloy of two materials, one of which is a metal and the other an insulator. Electric charge will be transferred from one side to the other only when the concentration of the conducting material (the metal) lies above the percolation threshold p_c. Hence one can see that percolation is part of the field of critical phenomena.

ACKNOWLEDGMENTS

The author wishes to thank Dr. D. Stauffer who suggested this research project, and to Dr. R. B. Pandey who provided the computer data. Their ready advice and support is appreciated.

REFERENCES

(1) Newman, M. and Schulman, L. S., Journal of Physics A, 14, 1735, (1981).

(2) Mitescu, C. and Rousseng, J., Annals of the Israel Physics Society, 5, 81, (1983).

(3) Wilke, S., Gefen, Y., Ilkovic, V., Ahorany, A., and Stauffer, D. preprint.

(4) Pandey, R. B., Stauffer, D., Physical Review Letters, 51, 527, (1983), and private communication.

FACULTY SPONSOR OF THIS PAPER

Dr. Dietrich Stauffer
Institute fur Theoretische Physik
Universität zu Köln
Zülpicher Strasse 77
5000 Köln 41
West Germany

TEMPERATURE INDUCED VALENCE TRANSITIONS IN $SmS_{1-x}P_x$ ALLOYS*

K.D. Aylesworth, D.M. Howarth, and M.L.Wallner
Department of Physics and Astronomy
University of Wisconsin-Stevens Point
Stevens Point, WI 54481

ABSTRACT

Cryogenic lattice parameter measurements on a series of $SmS_{1-x}P_x$ solid solutions reveal the narrow range of composition parameter x in which temperature induced valence transitions are observed. Evidence is presented which suggests that a single temperature characterizes the onset of valence change for alloys within this composition range. These results are compared to the more widely studied $Sm_{1-x}Y_xS$ solid solutions.

INTRODUCTION

Transitions between phases of a substance can be induced by applying an external pressure. For example, an applied pressure of 6.5 Kbar induces a discontinuous transition in samarium-sulfide from a black semiconducting phase to a golden metallic phase. During this transition, the structure of the material does not change, but there is a decrease in the lattice parameter of the face-centered-cubic lattice. (1) For any cubic crystal, the lattice parameter a is related to the crystal plane spacing d by the equation

$$d^{-2} = (h^2 + k^2 + l^2)\, a^{-2},$$

where (hkl) are the Miller indicies that locate the plane in the crystal. For a face-centered-cubic lattice, the Miller indices can only have integer values that are all even or all odd.

At first it was thought that this was a simple electronic transition from a cationic divalence to trivalence. More recent measurements of the lattice parameter and magnetic susceptibility suggest that the golden metallic phase material is characterized by a mixture of valence states. The average value of the valence is 2.8. This mixed valent compound has novel electric, magnetic and thermal properties.

Valence mixing in SmS also can be induced by chemical alloying with other rare-earth sulfides. Alloying with samarium pnictides can also induce transitions to intermediate valence phases. As a result, alloys such as ($Sm_{1-x}Y_xS$) and ($Sm\ S_{1-x}P_x$) have been investigated in recent years (3-6). It is typical to observe at the critical composition a first order transition from a divalent semiconducting phase to a mixed valent metallic phase at some particular temperature. As the temperature is lowered, the mixed valent phase appears. An interesting effect occurs at low temperatures for the mixed valent alloys near the critical composition. As the temperature is reduced, the gold phase crystals transform into a black powder with a corresponding increase in the lattice parameter. Upon warming up, the gold phase is again recovered, but at a slightly different temperature. Thus there is an apparent hysteresis effect when x is very close to the critical composition.

Cryogenic lattice parameter measurements on the $Sm_{1-x}Y_xS$ system (4) show that the temperature at which the lattice parameter expands is dependent upon the composition parameter x. For example, $Sm_{0.81}Y_{0.19}S$ expands without hysteresis at 185K while $Sm_{0.77}Y_{0.23}S$ expands at 160K. A similar effect occurs in $SmS_{1x}P_x$ alloys. The comparison of these two alloy samples is complicated by the fact that the temperature of the transition has hysteresis for x=0.06 (the critical composition) has has no hysteresis for x=0.08. It is therefore clear that if one is to eliminate the complication of hysteresis, one should investigate ($SmS_{1-x}P_x$) alloys with a composition parameter x larger than 0.08.

EXPERIMENTAL METHODS

Alloy samples of $SmS_{1-x}P_x$ with x=0.08, x=0.10, and x=0.12 were obtained from the University of Iowa. Sample

preparation techniques can be found elsewhere. (6)

Room temperature lattice parameters of these samples were obtained using a 114 mm Debye-Scherrer powder diffraction camera using Cu Kα radiation. A precision of ± 0.001 A was made possible by a computer analysis of nineteen pairs of diffraction lines separated by angles 4θ (θ is the angle of incidence of the X-ray beam on the crystal). Each pair of lines gave a measurement of the crystal plane spacing when used in the Bragg equation:

$$2d\sin(\theta) = \lambda .$$

The lattice parameters deduced from each pair of lines were fit by the method of least squares to the function

$$\frac{1}{2}\left(\frac{\cos^2\theta}{\sin\theta} + \frac{\cos^2\theta}{\theta}\right)$$

and an extrapolation to $\theta = 90°$ was used to give the most reliable result (7).

The low temperature lattice parameters were measured using an Air Products mini-cryostat designed for X-ray diffraction studies. Cooling was achieved by using the Joule expansion of compressed nitrogen gas. A temperature stability of ± 2K was typical.

The X-ray photographs taken with this mini-cryostat contain many intense diffraction lines that originate in the beryllium shroud that surrounds the sample and from the copper loaded grease this was used to bind the sample to the cold tip. These background lines obscured many of the diffraction lines coming from the sample in the back reflection region. Because of this interference, it was necessary to limit measurements to the hkl = (442) line for each temperature.

Under these conditions, the random errors resulted in an uncertainty in the lattice parameter of ± 0.002 Å. The systematic errors are larger than this number. Therefore each low temperature measurement was adjusted for relative comparison with the more precise room-temperature lattice parameter measurement.

RESULTS

The room-temperature lattice parameters obtained with the Debye-Scherrer camera are listed in Table I for the three alloy samples under investigation. These lattice parameters all agreed with those obtained by Henry, et. al. (6)

An estimate of the average samarium valence in these anion substituted alloys can be made by assuming a simple mixing of Sm^{2+}, Sm^{3+}, S^{2-}, and P^{3-}. The equation:

$$v(x) = 2 + x + \frac{(1-x)a(Sm^{2+}S) + xa(SmP) - a(x)}{a(Sm^{2+}S) - a(Sm^{3+}S)}$$

gives the room temperature valence v(x) for alloys of composition x and a(x) is the lattice parameter for the alloy. The lattice parameters for the known valence compounds are:

$$a(Sm^{2+}S) = 5.97 \text{ A}$$
$$a(Sm^{3+}S) = 5.62 \text{ A}$$
$$a(Sm\ P) = 5.77 \text{ A} .$$

The lattice parameter for the trivalent samarium sulfide was determined by an interpolation of the lattice parameters of the neighboring trivalent rare-earth sulfides (9). One can see from Table 1 that each alloy exhibits a considerable degree of valence mixing at room temperature.

$SmS_{1-x}P_x$ Sample	Room Temperature Lattice Parameter	Estimated Valence
x = 0.08	5.697 Å	2.81
x = 0.10	5.695 Å	2.83
x = 0.12	5.692 Å	2.85

TABLE I
Results of the diffraction measurements taken with the Debye-Scherrer powder diffraction camera. The valence estimates come from equation (4).

The results of cryogenic lattice parameter measurements of the two alloy samples are shown in Figure 1. The data for the $SmS_{0.92}P_{.08}$ sample fit a curve that decreases with cooling to 185 K and then rises sharply through the lowest temperature obtainable with this apparatus. The initial decrease

in the crystal dimension is expected with cooling. The subsequent increase in the crystal dimension indicates a transition to a lower average samarium valence. This behavior is consistent with previously reported measurements (6). The $SmS_{0.90}P_{0.10}$ alloy is found to undergo a nearly identical transition at 185 K as well. Larger random errors are evident in the cryogenic lattice parameters of this alloy because of difficulty encountered in centering the sample in the X-ray beam. The (442) line in this case appeared fainter than the corresponding line for the x=0.08 alloy. Within experimental uncertainty, low temperature lattice parameter measurements of Sm $S_{0.88}P_{0.12}$ failed to demonstrate any change in the average samarium valence down to 100K.

CONCLUSIONS

Results of the measurements on the x=0.12 alloy suggest that the composition interval over which temperature induced valence transitions are observed for Sm $S_{1-x}P_x$ (x=0.06 to 0.12) is quite narrow when compared with other mixed valent alloy systems. Henry, et.al. had previously shown that this type of valence transition was undetectable for x=0.20. Our results have narrowed the composition interval considerably.

The observation that a single temperature characterizes the onset of valence transitions in the $SmS_{0.92}P_{.08}$ and $SmS_{.90}P_{.10}$ alloys distinguishes $SmS_{1-x}P_x$ from $Sm_{1-x}Y_xS$. This difference may originate from the fact that yttrium substitution alters the cationic symmetry of mixed valent samarium while phosphorus substitution does not. Alterations in the local environment then would be much more pronounced in cation substituted systems.

The limited composition range available for investigation of this phenomenon in the $SmS_{1-x}P_x$ system makes it difficult to firmly conclude that the transition temperature is indeed constant. It appears desirable at this point to investigate other anion substituted systems such as $SmS_{1-x}As_x$. These may exhibit a broader composition range for temperature induced valence transitions.

ACKNOWLEDGMENTS

We are indebted to Professors William Savage and John Schweitzer at the University of Iowa who supplied the alloy samples used in this investigation. One of us (K.D.A) gratefully acknowledges the summer support provided by the Personnel Development Committee of the University of Wisconsin-Stevens Point.

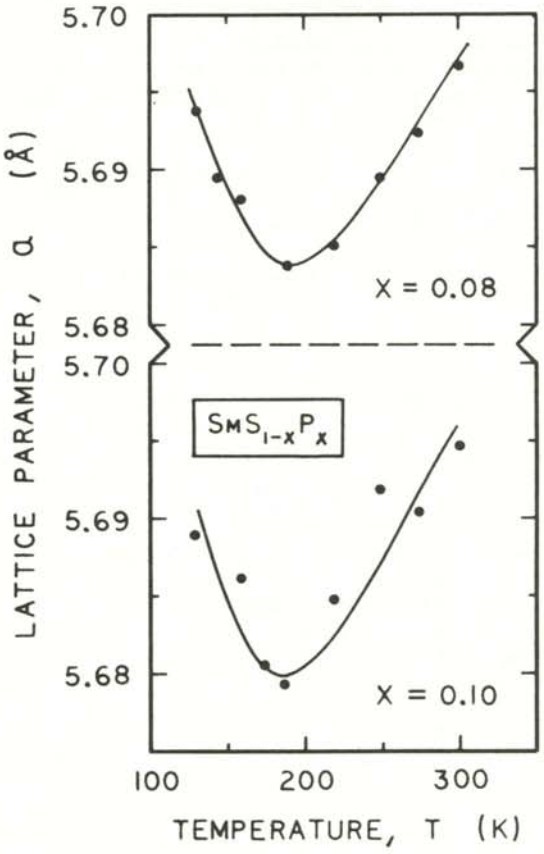

FIGURE I
Cryogenic lattice parameters for the solid solutions $SmS_{0.92}P_{0.08}$ and $SmS_{0.90}P_{.10}$ in the temperature interval 100k - 300K.

REFERENCES

* ...This work was supported by the National Science Foundation under grant PRM-8109738, by the Research Corporation under Cottrell Grant 8993, and by the Society of Physics Students under a 1982-83 Bendix Award.

(1) Jayaraman, V., Narayanamurti, V., Bucher, E., and Maines, R. G., Phys. Rev. Lett., 25, 1430 (1970).

(2) Maple, M. B. and Wohlleben, D., Phys. Rev. Lett. 27, 511 (1971).

(3) Penney, T. and Holtzberg, F., Phys. Rev. Lett., 34, 322 (1975).

(4) Tao, L. J., and Holtzberg, F., Phys. Rev. B 11, 3842 (1975).

(5) Dernier, P. D., Weber, W., and Longinotti, L. D., Phys. Rev. B 14, 3635 (1976).

(6) Henry, D. C., Sisson, K. J., Savage, W. R., Schweitzer, J. W., and Cater, E. D., Phys. Rev. B 20, 1985 (1979).

(7) Azaroff, L. V., Elements of X-ray Crystallography, McGraw-Hill, New York, 1968, p.477.

(8) Pollak, R. A., Holtzberg, F., Freeouf, J. L., and Easterman, D. E., Phys. Rev. Lett. 33, 820 (1974).

(9) Bucher, E., Andres, K., DiSalvo, F.J., Maita, J. P., Gossard, A.C., Cooper, A. S., and Hall, G. W. Jr., Phys. Rev. B 11, 500 (1975).

FACULTY SPONSOR OF THIS PAPER

Dr. R. B. Beeken
Department of Physics and Astronomy
University of Wisconsin
Stevens Point
Stevens Point, WI 54481

OPTICAL LEVITATION

Donn Michael Silberman *
Physics Department
University of Arizona
Tuscon, AZ 53233

ABSTRACT

Micron-sized drops of glycerol have been trapped and accelerated in a stable optical potential well provided by a focused beam from a continuous laser. The theory of how this works is presented in detail. An experiment is described that verifies the theory.

INTRODUCTION

The trapping and acceleration of micron-sized particles using the beam of a continuous laser was first reported by A. Ashkin (1) in 1970. Since that time, a number of papers have appeared on the subject.

The experiment described in this paper is similar to the Millikan Oil Drop experiment. In this case, instead of using an electric field to levitate an electrically charged drop as Millikan did, a radiation field, produced by a laser, is used to levitate an electrically neutral drop. This paper presents the theory of why a radiation field can be used to levitate a neutral drop and gives the details of an experiment that verifies it. This experiment is easily done where ever a 100 milliwatt laser is available.

THEORETICAL DEVELOPMENT

The geometry of the problem is shown in the ray diagram (Figure 1). The light ray is traveling normal to the earth's surface and is incident on a sphere that is partially transparent to that ray. The reflected and transmitted rays are shown. If the indicies of refraction

$$n(s) > n(m)$$

are known, the laws of reflection and refraction at the boundaries can be used to find the force imparted to the sphere by the incident light. This force (F_{rp}), which is due to the radiation pressure, must be greater or equal to the force of gravity (F_g) plus any viscous forces (F_v) acting on the sphere in order to trap or accelerate the sphere.

The force of gravity acting on the sphere is:

$$F_g = mg = 4/3\ \pi r^3 \rho g\ ,$$

where r is the radius of the sphere, ρ the density of the spherical oil drop, and g the acceleration due to gravity.

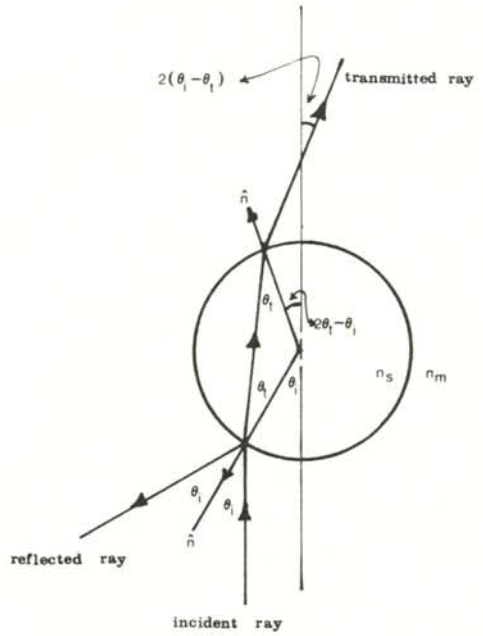

FIGURE 1
Ray diagram of the laser light as it passes through a spherical drop. The photons travel along the rays.

The viscous force acting will take on the form of Stokes Law:

$$\overline{F}_v = -6\pi r\eta\overline{v},$$

where η is the viscosity of the medium through which the drop is falling, and $\overline{v}$ is the velocity of the sphere. $\overline{F}_{rp}$ is equal to the sum of the vertical components of the forces due to the reflected and transmitted photons (the photon paths are represented by the rays).

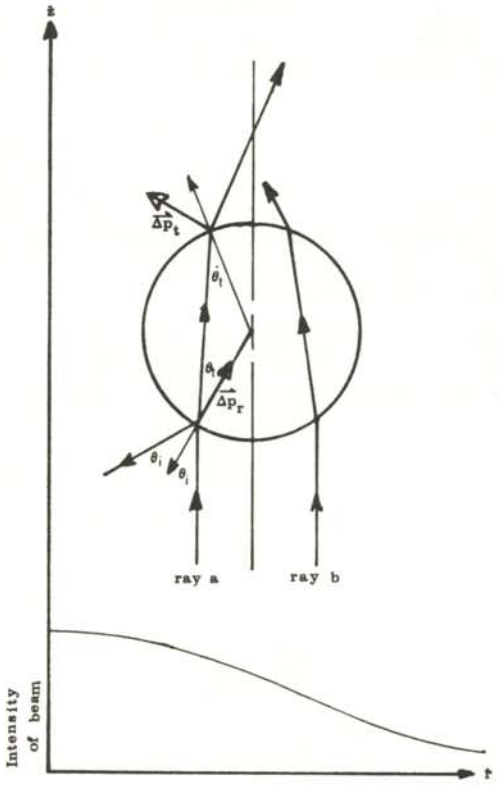

FIGURE 2
Momentum diagram of the light traveling through the drop. The drop is off the center line of the Gaussian distribution of the light intensity of the TEM_{00} mode of the Argon laser.

These forces are shown in Figure 2 as change-in-momentum vectors. The two rays "a" and "b" are incident on a sphere that is off the center axis of the Gaussian distribution of the light intensity of the TEM_{00} mode of the laser. The net effect is that the hemisphere closer to the beam axis receives a horizontal force toward the beam center, while the other hemisphere receives a positive vertical force. Since the beam intensity (number of incident photons/area/time) decreases with distance away from the beam axis, the net horizontal force is always acting towards the beam center. This means that the drops will track along the beam axis.

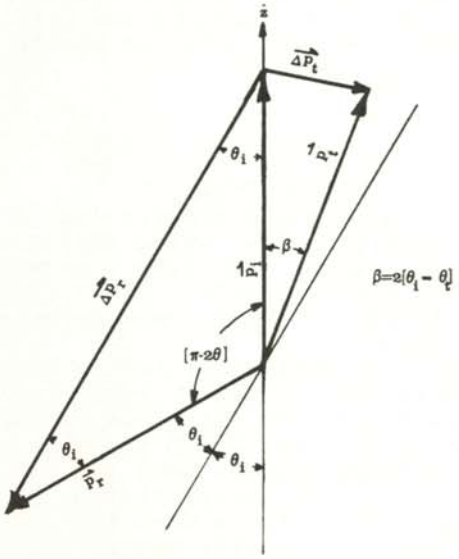

FIGURE 3
Vector momentum diagram for the laser light passing though the drop. These diagrams are used to find the z component of the force due to the radiation pressure.

Summing the z component of the forces due to the reflected photons (F_{rz}) and those due to the transmitted photons (F_{tz}) over the bottom half of the sphere gives:

$$\overline{F}_{rp} = \overline{F}_{tz} + \overline{F}_{rz} = \hat{z}\,N\left[(1-q)\int_0^{\pi/2}|\overline{\Delta P}_{tz}|\cos\theta_i\,d\beta + q\int_0^{\pi/2}|\overline{\Delta P}_{rz}|\cos\theta_i\,d\beta\right]$$

where N is the number of photons/area/time, q is the reflectance of the sphere, θ_i is the angle that the incident photon makes with the normal to the surface of the sphere $\hat{n}$, and $d\beta$ is the surface element. The incident momentum is given by:

$$\overline{P}_i = (h\nu/c)\hat{z}$$

where h is Planck's constant, ν the frequency, and c the speed of light. Using the ray diagram (Figure 1) and the vector diagram (Figure 3), the z

Transmitted	Reflected
$\overline{\Delta P_t} = \overline{P_t} - \overline{P_i}$	$\overline{\Delta P_r} = \overline{P_i} - \overline{P_r}$
to find z-component	to find z-component
$\lvert\overline{\Delta P_{tz}}\rvert = \lvert\overline{\Delta P_t}\rvert \sin(\theta_i - \theta_t)$	$\lvert\overline{\Delta P_{rz}}\rvert = \lvert\overline{\Delta P_r}\rvert \cos\theta_i$
$\lvert\overline{\Delta P_t}\rvert = 2\lvert\overline{P_i}\rvert \sin(\theta_i - \theta_t)$	$\lvert\overline{\Delta P_r}\rvert = 2\lvert\overline{P_i}\rvert \cos\theta_i$
$\lvert\overline{\Delta P_{tz}}\rvert = 2\lvert\overline{P_i}\rvert \sin(\theta_i - \theta_t)$	$\lvert\overline{\Delta P_{rz}}\rvert = 2\lvert\overline{P_i}\rvert \cos\theta_i$

component of the radiation pressure force becomes:

$$\overline{F^z_{rp}} = \hat{z}\, N \frac{h\nu}{c} 4\pi r^2 \left[(1-q)\int_0^{\pi/2} \sin^2(\theta_i - \theta_t)\sin\theta_i \cos\theta_i \, d\theta_i + q\int_0^{\pi/2} \cos^3\theta_i \, d\theta_i\right]$$

Snell's Law gives:

$$\theta_t = \arcsin\left[\, n(\text{medium})/n(\text{sphere})\sin\theta_i\right]$$

The value of the reflectance can be measured by placing the oil in a glass container and shining the laser on it. The ratio of the power reflected to the power incident is the value of q. Using our measured value of q, the value of the quantity in brackets in equation 2 becomes 0.116.

The force due to the radiation pressure can be written as:

$$\overline{F^z_{rp}} = \{N\ (h\nu/c)\ 4\pi r^2 Q\}\ \hat{z}$$

where Q is the value of the integrals in the square brackets. It should be noted that the effect of the internally reflected rays at the exiting boundary at the top of the drop are ignored. Their effect on the result is small.

If the beam has a cross-sectional area $=\pi\omega^2$ (which changes with the height because the beam is focused), the force can be written as:

$$\overline{F^z_{rp}} = 4PQr^2/c\omega^2\ \hat{z} = k/\omega^2\hat{z}$$

where ω is the radius of the beam and P is the total power in the incident beam.

In the region far below the focus waist (see Figure 4) at z=-2L, the velocity of the sphere is 0, so Newton's law tells us that the net force is zero. This means that

$$\overline{F^z_{rp}} = -\overline{F_g}$$

which becomes:

$$4PQr^2/c\omega^2 = 4/3\pi r^3\,\rho g$$

Hence the radius of the sphere that would be trapped is given by:

$$r = 3PQ/(c\omega^2\pi\rho g)$$

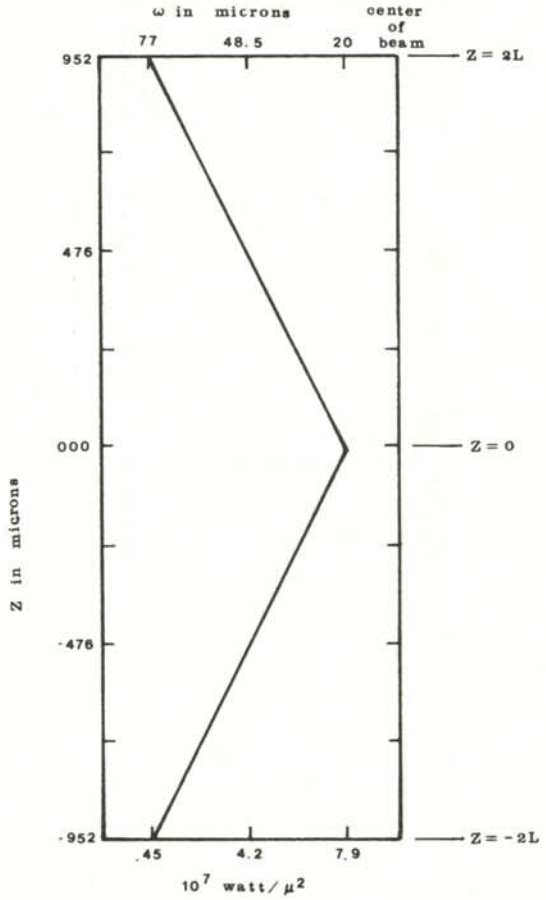

FIGURE 4
The geometry of the beam that was used to levitate the oil drops. The figure on the left is the power profile. The right figure is the spatial profile.

If the sphere obtains a small upward velocity, it will accelerate until it reaches z = -L/2 where terminal velocity is reached in accordance with Stoke's Law. To calculate the terminal velocity, one must remember that as the drop moves upward, the power/area changes. The

size of the beam is given by:

$$\omega_p = sz + \omega$$

where s is the slope of the diverging beam (see figure 4), and ω the radius of the focus at the waist (z=0). The

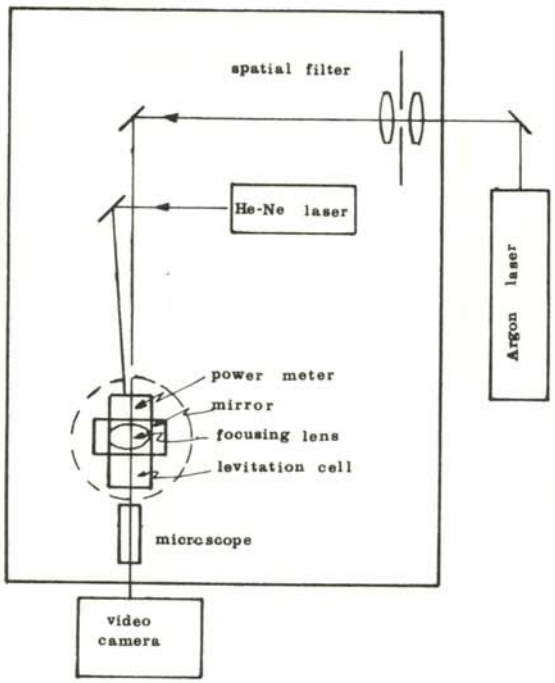

FIGURE 5
Experimental set-up for the optical levitation experiment.

velocity can be found using the energy balance integrals shown below. The energy put into the drop either goes into kinetic energy or gravitational energy.

$$\int_0^{L/2} \frac{k\,dz}{(sz+\omega_p)^2} = \int_0^{L/2} a\,v(z)\,dz + \int_0^{L/2} mg\,dz$$

where a is the coefficient in Stoke's Law.

The average velocity of the spheres in the central part of the focused beam (which can be measured) is given by:

$$\langle v\rangle = (1/L)\int_0^{L/2} v(z)\,dz$$

Performing these integrals gives the result:

$$\langle v\rangle = -\frac{8PQr^2}{Lca}\left[\frac{1}{s\left(\frac{sL}{2}-\omega_p\right)} - \frac{1}{s\omega_p}\right] - \frac{4\pi r^3 g\,\rho}{3a}$$

Everything in this equation is measurable. The aim of the experiment is to verify this result.

THE EXPERIMENT

A focused continuous laser beam (100 milliwatts power) is directed vertically into a glass cell in which glycerol drops may be sprayed from above. A properly calibrated viewing microscope is aligned horizontally to inspect the drops as they are trapped and accelerated near the focus of the beam. In the experiment reported here, the data were taken using a video-recorder as shown in Figure 5. Using the recorder allowed the data to be analyzed at leisure at a later time. A Helium-Neon laser was used to illuminate the calibration scale of the viewing microscope. This laser was used because its red color contrasted well with the blue light of the Argon laser used to levitate and illuminate the spheres. The brilliant scatter of the laser light off the drops can be seen easily by the unaided eye. The geometry of the beam (the slope s in equation 7) was measured by introducing smoke or water into the cell. The laser power was measured by the use of a power meter placed over the cell.

The average velocity was determined by measuring the time for the drop to move a distance of 476 microns. A total of 66 drops were tracked. The value of the slope of our beam was $(6.0\pm.5)\times10^{-3}$. The details of the laser beam profile are shown in Figure 4. Using oil of density (1256 ± 5)kg/m and reflectance q= $0.10\pm.01$ and a 100 milliwatt laser determined that the radii of the trapped drops were r=.50 ±.05 microns. Together these gave a predicted average velocity of

$$\langle v\rangle\,(\text{theory}) = (3.0\pm\beta)\times10^{-4}\,\text{m/sec}$$

This compares quite favorably with the measured value of:

$$\langle v\rangle\,(\text{experimental}) = (3.1\pm.4)\times10^{-4}\,\text{m/sec}.$$

CONCLUSION

The results obtained in this experiment support the theory developed as the experimentally measured velocity overlaps the theoretical value. The forces due to the focused laser light can trap and accelerate micron-sized

electrically neutral semi-transparent particles. The only special piece of equipment needed to do this experiment is the 100 milliwatt laser. The rest of the material is commonly available in the advanced undergraduate laboratory.

ACKNOWLEDGMENTS

The author wishes to thank Professor Wangsness for his wonderful book on Electromagnetic Fields and Professor Wing for teaching the course in the manner he did. He is indebted to Professor Stegeman for providing the laboratory in which the experiment was done. Finally, he wishes to thank Professor K. C. Hsieh for his support.

REFERENCES

* Present address:
Melles Griot
Laser Products Division
435 South Pacific St.
San Marcos, CA 92069

(1) Ashkin, A., Phys. Rev. Lett. 24, 156 (1970)

(2) Ashkin, A. and Dziedzic, J. M., Appl. Phys. Lett. 19, 283 (1971).

Ashkin, A., Scientific American 226, 63 (1972).

Ashkin, A., and Dziedzic, J. M., Phys. Rev. Lett. 39, 139 (1973).

Ashkin, A., and Dziedzic, J. M., Appl. Phys. Lett. 24, 586 (1974).

Ashkin, A., and Dziedzic, J. M., Science 187, 1073 (1975).

Ashkin, A., and Dziedzic, J. M., Appl. Phys. Lett. 28, 333 (1976).

Ashkin, A., and Dziedzic, J. M., Phys. Rev. Lett. 36, 267 (1976).

Ashkin, A., and Dziedzic, J. M., Appl. Phys. Lett. 30, 202 (1977).

Ashkin, A., and Dziedzic, J. M., Phys. Rev. Lett. 38, 1351 (1977).

Ashkin, A., "Applications of Laser Radiation Pressure", Science 210, 1081 (1980).

FACULTY SPONSOR OF THIS PAPER

Dr. K. C. Hsieh
Department of Physics
University of Arizona
Tuscon, AZ 53233

LAPLACE'S EQUATION, MICROCOMPUTERS, AND THE CLASSROOM

Jeanne A. Jackson
Department of Physics and Astronomy
Appalachian State University
Boone, NC 28608

ABSTRACT

Finding the solution to differential equations such as LaPlace's equation gives a teacher a good opportunity to familiarize students with one way in which computers are used in physics. Micro-computers are an excellent tool for this undertaking. One does not need a larger main-frame computer. This paper will present the Jacobi and alternating-direction-implicit methods for solving Laplace's equation. These methods will be compared in terms of accuracy, speed, and storage space requirements.

INTRODUCTION

LaPlace's equation,

$$\nabla^2\varphi = 0$$

occurs frequently in physics. In thermodynamics, the function φ gives the steady-state temperature distribution over a region. In fluid dynamics, it is the "velocity potential" of laminar, irrotational flow of an incompressible fluid, while in electromagnetism, φ is the electric potential in a region of space. Analytical solutions of LaPlace's equation are possible in some situations. If it is not possible to obtain the boundary conditions or the geometry of the region as some closed mathematical function, analytical solutions are very difficult or impossible. In such cases, one must look to numerical methods to solve the equation.

A number of methods for solving LaPlace's equation are best suited for use on large main-frame computers. The advent of the home computer has given rise to interest in methods that can work on systems that are slower and have less memory. These sort of limitations render some of the numerical methods unsuitable for use on the small computer.

Two different methods of numerically solving LaPlace's equation will be examined in this paper. Attention is given to the following characteristics: a) the accuracy of the method, b) the amount of memory needed to store and run the program, and c) the time it takes the process to reach a desired level of accuracy. The methods were written and run on a Commodore PET 4016 micro-computer with 15,359 words of memory available.

The two methods under consideration are Jacobi's method and the so-called alternating-direction-implicit (ADI) method.(1,2) Before comparing how they work, it may be beneficial to review the theory upon which the methods are based.

THEORETICAL BACKGROUND

Jacobi's method

The finite difference equation upon which Jacobi's method is based comes from a Taylor expansion of the function. The region in which the solution is desired is divided into a regular grid with $\Delta x = \Delta y = h$. (Figure 1) The Taylor expansion of the function $\varphi(x,y)$ about the points $(x\pm h, y\pm h)$ gives:

$$\left.\begin{aligned}
\varphi(x-h,y) &= \varphi(x,y) - h\frac{\partial\varphi}{\partial x} + \frac{h^2}{2}\frac{\partial^2\varphi}{\partial x^2} \\
\varphi(x+h,y) &= \varphi(x,y) + h\frac{\partial\varphi}{\partial x} + \frac{h^2}{2}\frac{\partial^2\varphi}{\partial x^2} \\
\varphi(x,y-h) &= \varphi(x,y) - h\frac{\partial\varphi}{\partial y} + \frac{h^2}{2}\frac{\partial^2\varphi}{\partial y^2} \\
\varphi(x,y+h) &= \varphi(x,y) + h\frac{\partial\varphi}{\partial y} + \frac{h^2}{2}\frac{\partial^2\varphi}{\partial y^2}
\end{aligned}\right\} O(h^2)$$

When the four terms are added together, the first derivative terms cancel out, resulting in the equation:

$$\frac{\partial^2\varphi}{\partial x^2} + \frac{\partial^2\varphi}{\partial y^2} = \frac{1}{h^2}\Big[4\varphi(x,y) - \varphi(x+h,y) - \varphi(x-h,y) - \varphi(x,y+h) - \varphi(x,y-h)\Big] + O(h^2)$$

where $O(h^2)$ means that as h becomes small, the error is proportional to h^2.

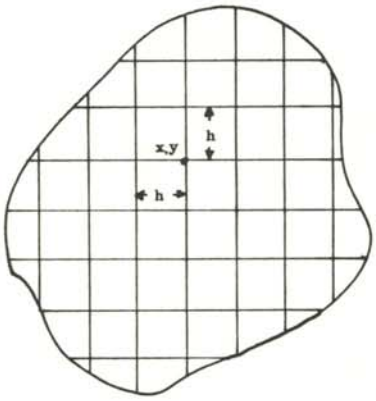

Figure 1
Grid mesh used to set up finite difference equations for the solution to LaPlace's equation.

LaPlace's equation then says that the left side of the equation must equal zero. This then results in the finite difference equation:

$$\varphi(x,y) = \frac{1}{4}\Big[\varphi(x+h,y) + \varphi(x-h,y) + \varphi(x,y+h) + \varphi(x,y-h)\Big]$$

which allows one to calculate the solution to LaPlace's equation at the point (x,y) if you know the values at the neighboring points. If each of the squares in Figure 1 is labeled by an integer, this algorithm for solving LaPlace's equation can be written as:

$$\varphi(i,j) = 1/4\big[\varphi(i+1,j) + \varphi(i-1,j) + \varphi(i,j+1) + \varphi(i,j-1)\big] \quad (1)$$

where i and j are integers.

The ADI method

To find the finite difference equations on which the ADI method is based, one again divides the region in the manner of Figure 1. Now one assumes that the function φ depends upon position and time and actually solves a diffusion equation:

$$\nabla^2\varphi = \frac{\partial\varphi}{\partial t}$$

The function $\varphi(x,y,t)$ is expanded using a Taylor series about the points $(x \pm h, y \pm h, t + \Delta t)$ and a finite difference solution for $\varphi(x,y,t+\Delta t)$ is found. The expansions to order h^2 are:

$$\varphi(x,y+h,t) = \varphi + h\frac{\partial\varphi}{\partial y} + \frac{h^2}{2}\frac{\partial^2\varphi}{\partial y^2}$$

$$\varphi(x,y-h,t) = \varphi - h\frac{\partial\varphi}{\partial y} + \frac{h^2}{2}\frac{\partial^2\varphi}{\partial y^2}$$

$$\varphi(x+h,y,t+\Delta t) = \varphi + h\frac{\partial\varphi(t+\Delta t)}{\partial x} + \frac{h^2}{2}\frac{\partial^2\varphi(t+\Delta t)}{\partial x^2}$$

$$\varphi(x-h,y,t+\Delta t) = \varphi - h\frac{\partial\varphi(t+\Delta t)}{\partial x} + \frac{h^2}{2}\frac{\partial^2\varphi(t+\Delta t)}{\partial x^2}$$

There are three parameters that can be varied: x position, y position, and time. We first choose to move in the y direction at time t and then the x direction at time t + Δt. Adding together the terms for this yields:

$$2\varphi + h^2\left[\frac{\partial^2\varphi}{\partial y^2} + \frac{\partial^2\varphi(t+\Delta t)}{\partial x^2}\right] + 2\varphi(t+\Delta t)$$

Notice that once again, the first derivative terms vanish. A rearrangement of these terms gives:

$$\frac{\partial^2\varphi}{\partial y^2} + \frac{\partial^2\varphi(t+\Delta t)}{\partial x^2} = \frac{1}{h^2}\Big[-2\varphi - 2\varphi(t+\Delta t) + \varphi(x,y+h,t) + \varphi(x,y-h,t) + \varphi(x+h,y,t+\Delta t) + \varphi(x-h,y,t+\Delta t)\Big]$$

Since Poisson's equation holds for this system, the expression on the left is equal to the partial derivative with respect to time. The Taylor expansion for the partial derivative with respect to time is:

$$\frac{\partial\varphi}{\partial t} = \Big[\varphi(t+\Delta t) - \varphi(t)\Big]\frac{1}{\Delta t} + O(\Delta t)$$

Keeping terms of order Δt results in the following relationship:

$$\varphi(x,y,t+\Delta t) = \frac{1}{\rho}\Big[\varphi(x,y+h,t) - 2\varphi(x,y,t) + \varphi(x,y-h,t) + \varphi(x+h,y,t+\Delta t) - 2\varphi(x,y,t+\Delta t) + \varphi(x-h,y,t+\Delta t)\Big]$$

where ρ is an iteration parameter whose value is:

$$\rho = h^2/\Delta t.$$

Now we step in the x direction at time t + Δt and the y direction at time

$t + 2\Delta t$. This process yields another equation for $\varphi(x,y,t+\Delta t)$:

$$\varphi(x,y,t+\Delta t) = \frac{1}{\rho}\Big[-\varphi(x,y,t+2\Delta t) + 2\varphi(x,y+h,t+2\Delta t) + \varphi(x,y-h,t+2\Delta t) + \varphi(x-h,y,t+\Delta t) - 2\varphi(x,y,t+\Delta t) + \varphi(x+h,y,t+\Delta t)\Big]$$

The two equations for $\varphi(x,y,t+\Delta t)$ must be simultaneously true if LaPlace's equation is to be true. Once again, if the squares in the region of interest are labeled by integers, this finite difference equation results in two equations:

$$\left.\begin{aligned} \varphi_{ij}^{n+1} &= \varphi_{ij}^{n} + \frac{1}{\rho}\Big[\varphi_{i+1j}^{n+1} - 2\varphi_{ij}^{n+1} + \varphi_{i-1j}^{n+1} + \varphi_{ij-1}^{n} - 2\varphi_{ij}^{n} + \varphi_{ij+1}^{n}\Big] \\ \varphi_{ij}^{n+1} &= \varphi_{ij}^{n+2} + \frac{1}{\rho}\Big[\varphi_{i+1j}^{n+1} - 2\varphi_{ij}^{n+1} + \varphi_{i-1j}^{n+1} + \varphi_{ij-1}^{n+2} - 2\varphi_{ij}^{n+2} + \varphi_{ij+1}^{n+2}\Big] \end{aligned}\right\} \quad (2)$$

The iteration parameter can be chosen to minimize the computing time.

WRITING THE PROGRAM

Jacobi's method

The finite difference equation 1 is used in a program in the following manner:

1. Define the geometry of the region of interest.
2. Define the boundary conditions
3. Compute the value of φ at all points within the boundary. One must know the values at every point on the boundary.
4. Check to see if the desired accuracy has been reached.
5. Repeat steps 3 and 4 until the desired accuracy is obtained.

As the outline indicates, the Jacobi method is quite simple to program. If there are any difficulties, they will be encountered in steps 1 and 2. There one establishes two two-dimensional arrays to hold the values of φ. These arrays contain the values of the boundary conditions and are used to store the old values and to calculate the new values. The accuracy is determined by comparing the two arrays to see if the values changed.

The ADI method

The ADI method involves two equations for each time step. As the name implies, the equations are first implicit in one direction (x) and then in the other (y). This is contrasted with the Jacobi method where the finite difference equation is implicit in both directions.

Applying Equation 2 to a problem results in a set of i equations for i unknowns. If represented in matrix form, they form a tridiagonal matrix. Such sets of equations can be solved using the Thomas algorithm. (2) Programming the Thomas algorithm is no easy matter. First, one rearranges the finite difference equations (Equation 2) so the terms in φ^n and φ^{n+1} are on opposite sides of the equations. Then one calculates a set of intermediate values a, b, c, d, β and γ. These values then can be put into an algorithm that will compute φ_i. The calculations are repeated until the desired accuracy is reached. The algorithm is as follows:

1. Put the finite difference equations in the form

$$a_i\varphi_{i-1} + b_i\varphi_i + c_i\varphi_{i+1} = d_i \qquad 1 \leqq i \leqq R \qquad a_1 = c_R = 0$$

2. Compute

$$\beta_i = b_i - (a_i c_i)/\beta_{i-1} \qquad \beta_1 = b_1/a_1$$

and

$$\gamma_i = (d_i - a_i\gamma_{i-1})/\beta_i \qquad \gamma_1 = d_1/b_1$$

3. Then calculate

$$\varphi_i = \gamma_i - (c_i\varphi_{i+1})/\beta_i \qquad \varphi_R = \gamma_R$$

4. Go on to the next i until you reach the end.

5. If you haven't reached the desired accuracy, repeat steps 2, 3, and 4.

Listing of BASIC programs written for these two methods to work on the Commodore PET 4016 can be obtained by writing the Physics Department.

COMPARISON OF TECHNIQUES

The best way to evaluate numerical methods is to compare their performance on a problem. The problem used is outlined below. A rectangular plate has temperature 0 at all points on its surface. A heat source is applied to the plate that keeps the temperature

along each edge constant. The steady-state temperature distribution on the surface is given by LaPlace's equation. The answer to the problem is obvious, so the accuracy can be checked. The surface is divided into a 10 x 10 grid.

Accuracy

Both systems shown here are second-order correct. Therefore, the relative accuracy of the two methods is not a determining factor in the decision of which one to use.

Speed

The Thomas algorithm (used in the ADI method) calculates only one value of φ per iteration for each grid point. Each of these calculations involves the determination of three intermediate quantities. The computer must do four calculations per grid point per iteration. Jacobi's method, on the other hand, requires the averaging of the values of φ at the surrounding points in order to calculate φ at one point during one iteration. This will be at least two or more calculations. Thus the determining factor as far as the speed is concerned will be the number of iterations needed to reach the desired level of accuracy.

When applied to this problem, the Thomas algorithm ran much faster than the Jacobi method. It reached two decimal place accuracy is less than one minute, while the takes over 11 minutes to achieve that level of accuracy in just 69 of the 100 points when the Jacobi method is used.

Space Used

The Jacobi method has the space advantage over the Thomas algorithm. The latter requires 4 arrays to store the values of φ and the intermediate variables, while the Jacobi method only requires two. In this example, the Thomas method required 3567 words of memory while the Jacobi method required only 2890 words.

Other Comparisons

The Jacobi method can be used to model time dependent processes. This is particularly effective if the output is formatted to correspond to the shape of the region in question. If one outputs the values of each iteration, the resulting propagation of values through the arrays will "mimic" a time dependent (diffusive) process.

The Jacobi method can be programmed to take advantage of the symmetry of a problem, perhaps reducing the number of calculations and hence the run time. This is impossible when one uses the Thomas algorithm. However, the speed of the Thomas algorithm is so great that any gain in efficiency due to symmetry probably would not make the Jacobi method more attractive from this standpoint.

CONCLUSIONS

Jacobi's method and the ADI method both successfully solve LaPlace's equation. Each method has intrinsic advantages and disadvantages. The ADI method runs faster by virtue of the Thomas algorithm, but this advantage may be somewhat offset by the larger amount of space it requires. Jacobi's method is much more conserving of space at the expense of time.

REFERENCES

(1) Gerald, Curtis F., Applied Numerical Analysis, Addison-Wesley Publishing Co. Reading, MA, 1970.

(2) von Rosenberg, Dale U., Methods for the Numerical Solution of Partial Differential Equations, American Elsevier Publishing Co., Inc. New York, 1969.

FACULTY SPONSOR OF THIS PAPER

Dr. David K. Monroe
Department of Physics and Astronomy
Appalachian State University
Boone, NC 28608